JOURNAL OF THERMOPHYSICS AND HEAT TRANSFER
Vol. 7, No. 2, April–June 1993

Magnetic Field Effects on the Computed Flow over a Mars Return Aerobrake

Grant Palmer*
NASA Ames Research Center, Moffett Field, California 94035

A numerical algorithm is developed to calculate the electromagnetic phenomena simultaneously with the fluid flow in the shock layer over an axisymmetric blunt body in a thermal equilibrium, chemical nonequilibrium environment. The flowfield is solved using an explicit time-marching, first-order spatially accurate scheme. The electromagnetic phenomena are coupled to the real-gas flow solver through an iterative procedure. The electromagnetic terms introduce a strong stiffness, which was overcome by using significantly smaller time steps for the electromagnetic conservation equation. The technique is applied in calculating the flow over a Mars return aerobrake vehicle entering the Earth's atmosphere. For the case where no external field is applied, the electromagnetic effects have little impact on the flowfield. With the application of an external magnetic field of 0.05 to 0.1 T, the solution indicates an increase in stagnation line shock standoff distance, wall pressure, and radiative heat transfer and a decrease in convective heat transfer.

Nomenclature

B = magnetic induction, T
c_s = species mass fraction
c_∞, T_∞, ρ_∞ = freestream speed of sound, temperature, density
D_{ij} = binary diffusion coefficient
E = electric field, V/m
e = total energy
$\bar{e}$ = charge per electron, 1.601×10^{-19} C
e_v = vibrational energy
h_s = species enthalpy, J/kg
j = current density, A/m^2
k = Boltzmann's constant, 1.3805×10^{-23} J/K
l_{ref} = grid scaling reference length
M = molar mass
n_e = electron number density
p = pressure
p_e = electron pressure, $n_e k T_e$
q_j = heat conduction
R = universal gas constant
T = translational temperature
Tv = vibrational temperature
t = time
u, v = velocity
u_s, v_s = diffusion velocity
$\bar{w}_s$ = chemical source term
X_s = species mole fraction
x, y = Cartesian coordinates
β = real-gas parameter
$\bar{\eta}$ = resistivity, Ω-m
μ_0 = permeability in a vacuum, $4\pi \times 10^{-7}$ h/m
ρ = density
Σ_m = summation considering only molecules
σ = conductivity, $1/\bar{\eta}$
τ_{ij} = shear stress

Introduction

RECENTLY, Mars mission plans have been proposed using aerobrakes that reach velocities during their re-entry into Earth's atmosphere in excess of 12 km/s. In a previous study,[1] flow around a Mars return aerobrake conducting a single pass direct entry in the Earth's atmosphere was analyzed. The vehicle has a lift/drag (L/D) of 0.5 and a ballistic coefficient of 300 kg/m^2.

Most computational studies of chemically reacting flow have assumed the gas to be, at most, weakly ionized.[2–4] This allows certain simplifications to the governing equations. The conductivity of air is assumed to be small, so that electromagnetic effects, such as electric and magnetic fields, can be removed from the conservation of momentum and energy equations.

In Ref. 1, flow was computed over the aerobrake traveling at 13.2 km/s at 64.8-km altitude, flight conditions close to the undershoot boundary, and near the point of peak heating. Peak ionization levels along the stagnation line exceeded 25%, clearly a significant level. Electromagnetic effects might have to be included in the physical model for these types of flows.

Much of the work on coupling the electromagnetic and fluid dynamic equations has concerned magnetohydrodynamic (MHD) flow computations.[5–7] Steady versions of the governing equations are solved under certain MHD flow approximations. Shebalin[8] coupled the electromagnetic and fluid dynamic equations. He found that plasmadynamic effects induced by the shock layer significantly influenced the temperature and density profiles even at velocities as low as 9 km/s. However, he used a simplified physical model and a quasi-one-dimensional test problem, therefore, his conclusions have not been tested using the full conservation equations to solve the flow over a blunt body at realistic flight conditions.

A great deal of work was done in the late 1950s and 1960s on the effects an externally applied magnetic field might have on a hypersonic flowfield.[9–14] Because of the lack of computational resources at that time, these studies used analytic methods over simple bodies with assumptions such as the Newtonian approximation. Their objective was to ascertain if an externally applied magnetic field could be used to decrease heat transfer to a vehicle. They found that shock standoff distance did increase, but could not quantitatively analyze their impact on pressure, temperature, and velocity values behind the shock.

In this study, modern computational fluid dynamic (CFD) techniques are used to couple the time-dependent Maxwell's equations to the Navier-Stokes equations, and to gauge the effect of both self-generated and externally applied magnetic fields on the computed flowfield. The magnetic induction is computed and the appropriate magnetic induction terms are added to the momentum and energy equations.

Presented as Paper 91-1462 at the AIAA 22nd Fluid Dynamics, Plasma Dynamics, and Lasers Conference, Honolulu, HI, June 24–26, 1991; received Jan. 17, 1992; revision received May 29, 1992; accepted for publication June 3, 1992.

*Research Scientist, Aerothermodynamics Branch. Member AIAA.

Governing Equations

The axisymmetric Navier-Stokes equations, including species continuity equations, represent the conservation of mass, momentum, and energy. They consist of a mass conservation equation for each species considered[15]:

$$\frac{\partial \rho_s}{\partial t} + \frac{\partial}{\partial x_j}(\rho_s u_j) + \frac{\hat{H}}{y} = -\frac{\partial}{\partial x_j}(\rho_s u_{sj}) + \bar{w}_s \tag{1}$$

a total mass conservation equation

$$\frac{\partial \rho}{\partial t} + \frac{\partial}{\partial x_j}(\rho u_j) + \frac{\hat{H}}{y} = 0 \tag{2}$$

two global conservation of momentum equations

$$\frac{\partial}{\partial t}(\rho u_i) + \frac{\partial}{\partial x_j}(\rho u_i u_j) + \frac{\partial p}{\partial x_i} + \frac{\hat{H}}{y} = \frac{\partial \tau_{ij}}{\partial x_j} + (j \times B)^i \tag{3}$$

and a total energy conservation equation

$$\frac{\partial e}{\partial t} + \frac{\partial}{\partial x_j}[(e + p)u_j] + \frac{\hat{H}}{y} = \frac{\partial q_j}{\partial x_j} + \frac{\partial}{\partial x_j}(u_i \tau_{ij}) + (E \cdot j) \tag{4}$$

where

$$\tau_{xx} = \frac{2}{3}\mu\left(2\frac{\partial u}{\partial x} - \frac{\partial v}{\partial y} - \frac{v}{y}\right)$$

$$\tau_{xy} = \mu\left(\frac{\partial u}{\partial y} + \frac{\partial v}{\partial x}\right)$$

$$\tau_{yy} = \frac{2}{3}\mu\left(2\frac{\partial v}{\partial y} - \frac{\partial u}{\partial x} - \frac{v}{y}\right)$$

Electromagnetic terms have been included in the momentum and energy conservation equations.[16,17] B can be either the self-generated magnetic field generated by electron pressure and temperature gradients in the flowfield or an externally applied field. The axisymmetric source vector $\hat{H}$ in the above equations has elements

$$\hat{H} = \begin{bmatrix} \rho_1(v + v_1) \\ \vdots \\ \rho_s(v + v_s) \\ \rho v \\ \rho u v - \tau_{xy} \\ \rho v^2 - (\tau_{yy} - \tau_{\theta\theta}) \\ (e + p)v + q_y - u\tau_{xy} - v\tau_{yy} + \sum_s h_s \rho_s v_s \end{bmatrix}$$

The determination of the diffusive mass flux follows a modified form of that presented by Curtiss and Hirschfelder[18]

$$\rho_s u_{sj} = -\rho \frac{1 - c_s}{\sum_{j \neq i}(x_j/D_{ij})} \mathrm{d}_{sj} - D_i^T \frac{\partial \ln T}{\partial x_j} \tag{5}$$

where

$$\mathrm{d}_{sj} = \frac{\partial c_s}{\partial x_j} + c_s\left(1 - \frac{m_s}{m}\right)\frac{\partial \ln p}{\partial x_j} - \frac{c_s}{p}\left(\frac{\rho}{m}F_i - \frac{m_i}{m}\sum n_k F_k\right) \tag{6}$$

The first term in Eq. (6) is the contribution due to species concentration gradients. The second term is the contribution due to pressure gradient. The third term is the contribution due to electrostatic forces, called forced diffusion. Forced diffusion is important only where there is significant charge separation.[19] In this study, the flow is considered to be locally charge neutral. The ambipolar phenomena are neglected because electromagnetic phenomena are not likely to be affected by these effects. When pressure and thermal effects were incorporated into the code, their effects were found to be small in both the stagnation and shoulder regions, so they were removed from the physical model.

The heat conduction is given by

$$q_j = -\kappa \frac{\partial T}{\partial x_j} + \sum_s \rho_s u_{sj} h_s \tag{7}$$

The determination of viscosity and thermal conductivity of the 11 species gas mixture follows the method of Gupta et al.[20]

At 13.2 km/s and 64.8-km altitude, the flow behind the shock wave can be assumed to be in near-thermal equilibrium.[19] There would be a small region immediately behind the shock where thermal nonequilibrium phenomena would be present. However, in the density range considered in the present work, this thermal nonequilibrium region would be small.[21] Translational temperature can be obtained from the equation relating the total energy and translational temperature:

$$e = 1.5RT\sum_s \frac{\rho_s}{M_s} + RT\sum_m \frac{\rho_s}{M_s} + e_v + e_{el} + \frac{1}{2}\rho(u^2 + v^2 + w^2) + \sum_s \rho_s h_s^0 \tag{8}$$

Pressure can be related to the other global conservation quantities by the relation

$$p = (\beta - 1)[e - \tfrac{1}{2}\rho(u^2 + v^2 + w^2)] \tag{9}$$

The quantity, β, used in the flux splitting, is defined as the ratio of specific static enthalpy to specific internal energy with a reference temperature of 0 K. For a perfect gas, β becomes the ratio of specific heats, γ.

Electromagnetic Terms

The magnetic induction, current density, and electric field in Eqs. (3) and (4) can be found by solving Maxwell's equations. Assuming local charge neutrality they are

$$\nabla \cdot j = 0 \tag{10}$$

$$\frac{\partial B}{\partial t} = -\nabla \times E \tag{11}$$

$$j = [(\nabla \times B)/\mu_0] \tag{12}$$

$$\nabla \cdot B = 0 \tag{13}$$

The generalized Ohm's law is expressed as

$$E = \bar{\eta} j - (u \times B) + (1/n_e \bar{e})(j \times B) - (1/n_e \bar{e})\nabla p_e \tag{14}$$

and is the conservation of electron momentum equation where terms involving electron density and shear stress are neglected.

The axisymmetric formulation of the governing equations results from the three-dimensional equations expressed in cylindrical coordinates where the velocity and gradients in the circumferential or Θ direction are zero. This leads to some important simplifications of Maxwell's equations. Writing out the three components of Eq. (11) with the axisymmetric simplifications

$$\frac{\partial B_x}{\partial t} = -\frac{E_\Theta}{y} - \frac{\partial E_\Theta}{\partial y} \tag{15}$$

$$\frac{\partial B_y}{\partial t} = \frac{\partial E_\Theta}{\partial x} \tag{16}$$

$$\frac{\partial B_\Theta}{\partial t} = \frac{\partial E_x}{\partial_y} - \frac{\partial E_y}{\partial_x} \tag{17}$$

The axisymmetric magnetic induction equations are thus decoupled such that B_x and B_y depend only on E_Θ, and B_Θ depends only on E_x and E_y.

Determination of the resistivity follows the method of Spitzer[22] and Delcroix[23]

$$\bar{\eta} = 65.3\lambda T_e^{-1.5} \tag{18}$$

where

$$\lambda = \log\left[(1.89506 \times 10^{16} T_e^{3.45})/n_e^{1.15}\right]$$

is a modified form of that presented by Braginskii.[17] Under thermal equilbrium conditions, the translational temperature is used to evaluate Eq. (18).

Self-Generated Magnetic Fields

The determination of the governing equations for self-generated magnetic fields follows that of Shebalin.[8] The last term in Eq. (14), called the thermoelectric term, acts as a source term for the generation of a magnetic field. Since circumferential gradients are zero for axisymmetric flow, the thermoelectric term is absent from the E_Θ component of Eq. (14). Thus, there is no mechanism for E_Θ, and subsequently, B_x and B_y to develop. Additionally, Eq. (11) indicates that E_Θ is zero when the system reaches steady state. Therefore, for axisymmetric flow with no applied magnetic fields, only the B_Θ component of magnetic induction need be considered. The magnetic field lines travel in circles around the x axis.

By combining Eqs. (17), (14), and (12), a nondimensional conservation equation for B_Θ can be written as

$$\begin{aligned}\frac{\partial B_\Theta}{\partial t} + \frac{\partial B_\Theta u}{\partial x} + \frac{\partial B_\Theta v}{\partial y} &= \frac{\partial}{\partial x}\left(\bar{\eta}\frac{\partial B_\Theta}{\partial x}\right) \\ &+ \frac{\partial}{\partial_y}\left(\bar{\eta}\frac{\partial B_\Theta}{\partial y}\right) + \frac{\partial}{\partial y}\left(\bar{\eta}\frac{B_\Theta}{y}\right) \\ &+ K_{pe}\left(\frac{\partial \not{\rho} p_e}{\partial y}\frac{\partial T_e}{\partial x} - \frac{\partial \not{\rho} p_e}{\partial x}\frac{\partial T_e}{\partial y}\right) + \frac{1}{2}\frac{\partial}{\partial x}\left(\frac{1}{n_e}\frac{\partial B_\Theta^2}{\partial y}\right) \\ &- \frac{1}{2}\frac{\partial}{\partial y}\left(\frac{1}{n_e}\frac{\partial B_\Theta^2}{\partial x}\right) + \frac{1}{y}\frac{\partial}{\partial x}\left(\frac{B_\Theta^2}{n_e}\right)\end{aligned} \tag{19}$$

where

$$K_{pe} = (KT_\infty/\bar{e}c_\infty^2 l_{\text{ref}}\sqrt{\mu_0\rho_\infty})$$

Applied Magnetic Field

Another set of assumptions that is consistent with Eqs. (10–14) is to assume that current density only exists in the circumferential direction. This says that current flows in circles about the x axis. $\nabla \cdot j = 0$ is thus always maintained. To satisfy Eq. (12), B_Θ must be zero. All three components of the electric field are assumed to be zero. The current density can then be expressed as

$$j_\Theta = \frac{1}{\mu_0}\left(\frac{\partial B_y}{\partial x} - \frac{\partial B_x}{\partial y}\right) = \sigma(uB_y - vB_x) \tag{20}$$

where the conductivity σ is the inverse of the resistivity.

The preceding assumptions were utilized in Refs. 9–14. The freestream conductivity and current density are assumed to be zero. The applied B field should decrease with increasing distance from the source and the B_y component should go to zero along the x axis. One relation that satisfies these constraints is

$$B_x = \frac{B_0(-2x^2 + y^2)}{(x^2 + y^2)^{5/2}}, \qquad B_y = \frac{-3B_0 xy}{(x^2 + y^2)^{5/2}} \tag{21}$$

This is the field from a dipole located at the origin. Behind the bow shock where the conductivity and current density are nonzero, the magnetic field is obtained from solution of Eq. (20) under the constraint of Eq. (13).

Chemical Model

The 30 chemical reactions used in this study were taken from Park.[24] Eleven species, N, N_2, O, O_2, NO, N^+, N_2^+, O^+, O_2^+, NO^+, and e^-, were considered. The forward and backward reaction rates are of the form

$$k_f(T) = C_f T^{\eta_f} e^{-\theta_d/T}, \qquad k_b(T) = [k_f(T)/K_{eq}(T)] \tag{22}$$

The reaction rate constants in Eq. (22) were obtained from Park.[24] If thermal equilbrium is assumed, the forward and backward reactions are always a function of the translational temperature.

Solution Algorithm

The presence of strong flow gradients such as shocks requires the use of some form of upwind differencing to maintain stability during the flow computation. The differencing technique used in the present algorithm is that of Van Leer flux-vector splitting.[25] The technique splits and differences the inviscid fluxes according to the direction of signal propagation. The solutions presented in this article were computed using first-order spatial differencing of the inviscid fluxes. However, the inclusion of second-order differencing is a relatively simple procedure using transition operators.[26]

The numerical solutions were all impulsively started, i.e., initially the flow was freestream everywhere. Freestream values were maintained along the supersonic inflow boundary. The outflow boundary was also assumed to be supersonic, and zeroth-order extrapolation from the interior was used. The no-slip condition and zero normal pressure gradient were imposed on the wall. A fixed wall temperature of 3300 K was maintained on the the body surface, which was assumed to be noncatalytic. This temperature is representative of possible heat shield materials. For the self-generated magnetic field case, the circumferential magnetic field was set to zero along the inflow boundary. The body surface was assumed to be an insulator, so current density along the body was zero for both the self-generated and externally applied magnetic field cases.

The governing equations are solved using an explict formulation. Normally, the inclusion of species continuity equations with source terms derived from finite-rate chemical reactions renders an explicit algorithm stiff, meaning that prohibitively small time steps are required to maintain stability. However, in previous studies[26,27] a technique was developed that overcomes this stiffness problem. Essentially, it scales the species mass fraction updates obtained after each iteration so that the largest change in any species mass fraction is no larger than a certain prescribed value. The method has successfully computed flows over a wide range of freestream conditions and has been corroborated with comparisons against both experimental data and computations using other explicit and implicit techniques.[2,26,27]

Equation (19) looks similar in form to the gasdynamic conservation equations. It contains convective terms, such as $\partial B_\Theta u/\partial x$, and diffusive terms, such as $\partial/\partial x[\bar{\eta}(\partial B_\Theta/\partial x)]$. The thermoelectric term acts as a source term for magnetic induction.

Solution of the time-dependent magnetic induction conservation equation proceeds exactly as the solution of the

Navier-Stokes equations. The convective terms are differenced using flux-vector splitting. The diffusive terms are differenced using a standard three-point stencil. Cross-derivatives are central-differenced.

The magnetic induction equation is stiffer than the other conservation equations. A time-step 10^4 times smaller than that used for the Navier-Stokes equations was found to be necessary to maintain stability. However, the magnetic induction equation converges faster than the Navier-Stokes equations for a given time increment. The induction equation was loosely coupled to the gasdynamics such that 100 iterations of the magnetic induction equation were executed using the smaller time step for every gasdynamic iteration. Values of velocity, electron pressure, and temperature passed to the electromagnetic subroutine are held constant during the 100 iterations. The updated values of current density and magnetic induction are used to evaluate the electromagnetic terms in the momentum and energy equations. This loose coupling avoids the prohibitive time step restrictions encountered with the fully coupled explicit technique, as well as the complexity and difficulty of a fully coupled implicit code.

For the applied magnetic field case, the current density is obtained by solving Eq. (20) using Gauss-Seidel relaxation under the constraint that Eq. (13) must also be obeyed. In the freestream and along the body, where there is no current density, the magnetic field is specified by Eq. (21).

Results

The Mars return aerobrake vehicle, first proposed by Tauber,[1] is shown in Fig. 1a. Designed for a lift-drag ratio of 0.5, it consists of a raked 45-deg half-angle cone blunted by a 0.8-m radius sphere. The rake angle is 67 deg. The top shoulder is rounded by a 0.45-m radius circle and the bottom shoulder by a 0.6-m radius circle. The vehicle is nearly symmetric, so the axisymmetric approximation is reasonable. The computational domain is also shown in Fig. 1.

Flow was computed over the vehicle traveling at 13.2 km/s at an altitude of 64.8 km, corresponding to one of its flight trajectory points. Figure 2 presents profiles of temperature and species distributions computed for these conditions. This represents the starting solution for the electromagnetic effects study. Figures 2a and 2c show temperature profiles along the stagnation line and near the shoulder. Figures 2b and 2d show species mole fractions. The gas is nearly completely dissociated behind the shock, both along the stagnation line and near the shoulder. The level of ionization in the stagnation is around 25%. The sharp rise in the atomic nitrogen mole fraction along the stagnation line near the body is due to the drop in both the ions and electron mole fractions in this region. Recombination increases the stagnation line mole fraction of N_2 from virtually zero in most of the shock layer to 0.04 at the wall. The stagnation line shock standoff distance is approximately 4.1 cm from the body. The region of nonequilibrium behavior, characterized by the temperature spike, extends for 0.6 cm behind the shock or 14.6% of the shock standoff distance. Behind this region, the temperature relaxes to an equilibrium value of around 12,750 K.

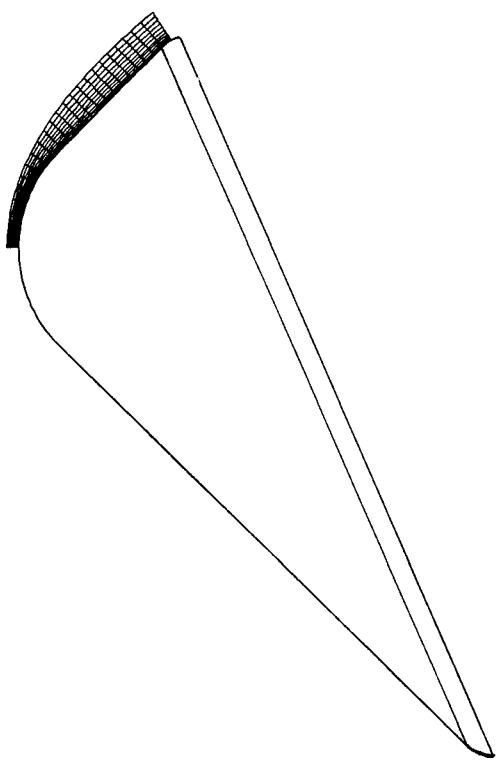

Fig. 1 Mars return aerobrake and computational domain.

Comparison to experiment in this flow regime is difficult due the high velocities, but some validation is possible. Using a shock tube, Wilson[28] observed the behavior of electron density for shock velocities of 9–12 km/s. Two of the quantities produced by Wilson's work are postshock electron number density and ionization distance.

The code was run over the aerobrake at a lower speed, 11.25 km/s, to compare the stagnation line electron number density profile against previous experimental[28] and computational[21] results. The value of peak electron number density computed by the present code compared closely with those found by Refs. 21 and 28, although the slope of the profile was steeper behind the shock. This may be due to thermal nonequilibrium effects not accounted for that are important at 11.25 km/s.

Ionization distance is obtained by fitting a straight line to the N_e^2 profile until it intersects the peak value. The distance from this intersection to the point the electron number density first starts to rise is the ionization distance. Wilson plotted experimentally observed values of ionization distance divided by freestream mean free path for shock speeds ranging from 9 to 12.5 km/s. Figure 3 shows these values along with those calculated by Park using the NONEQ code.[21] The code described in this study computed a value of 14.5 for the 13.2 km/s. As seen in Fig. 3, this value corresponds closely to those found by Park, and are consistent with the ionization distances seen experimentally.

Effects of Self-Generated Magnetic Induction

Self-generated magnetic induction occurs in an ionized—but charge-neutral—flowfield from gradients in the electron pressure and temperature. Looking at the thermoelectric term in Eq. (19), the generation of the circumferential component of magnetic induction, or B_Θ, is only possible if there are gradients in electron pressure and temperature in both the x and y directions. Therefore, the field strength should be zero along the stagnation line. The largest values of magnetic induction should occur in regions of expansion.

Figure 4 shows circumferential magnetic induction contours around the Mars return aerobrake. The peak value of magnetic induction is 1.86 G and occurs near the shoulder of the vehicle. Another local maximum occurs when the flow expands around the nose. Along the flat part of the aerobrake, between the nose and the shoulder, the induction is low, due to the reduced ξ derivatives of electron pressure and temperature in this region.

The inclusion of electromagnetic terms into the governing equations has virtually no effect on temperature, shock standoff, or any of the other flow quantities. This is not surprising since the maximum magnetic energy, B_Θ^2/μ_0 of 2.81×10^{-2} J/m^3 is seven orders of magnitude smaller than the total energy, 1.60×10^5, at the corresponding grid point. Even when the computed values of B_Θ were multiplied by a factor of 10, no appreciable difference was seen in the other flow quantities.

The contours levels shown in Fig. 4 exhibit some local minima, particularly near the nose of the body. This is due to the

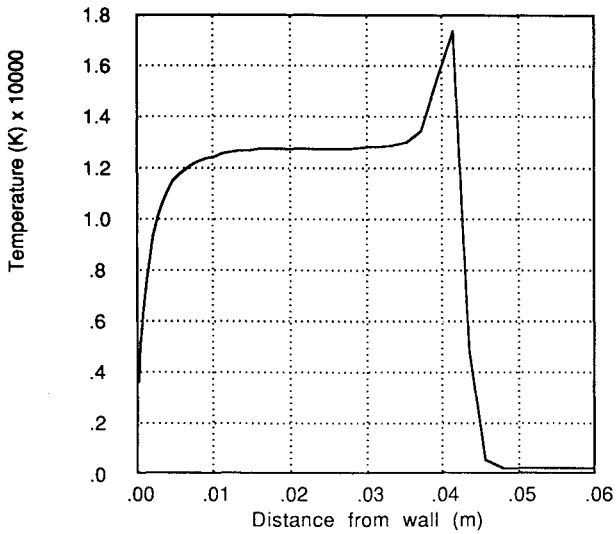

a) Stagnation line temperature profile

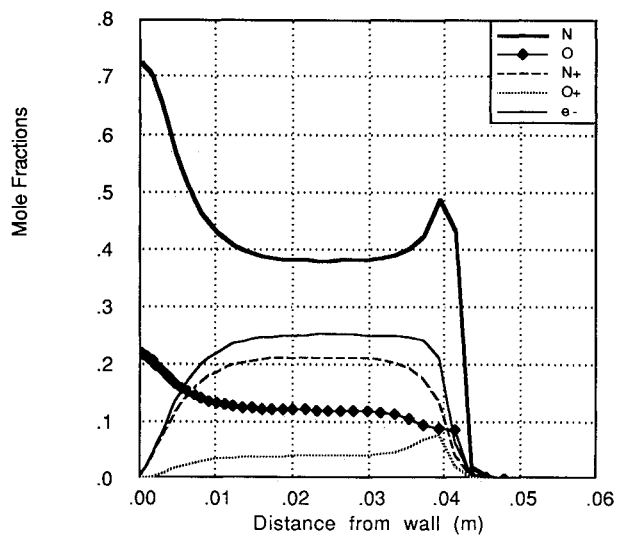

b) Stagnation line species distribution

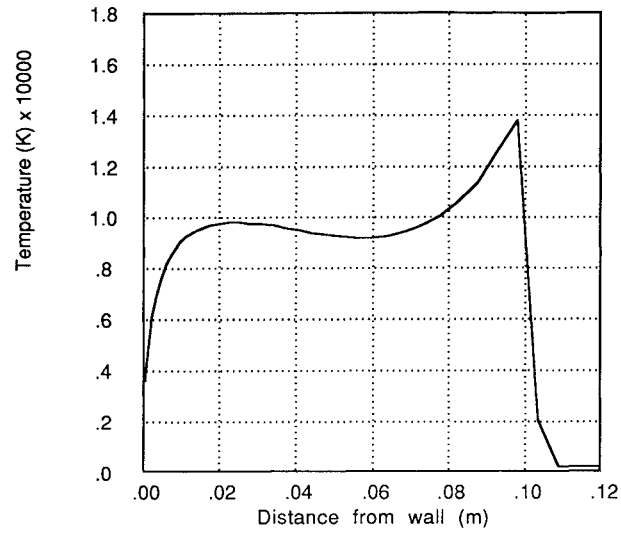

c) Shoulder region temperature profile

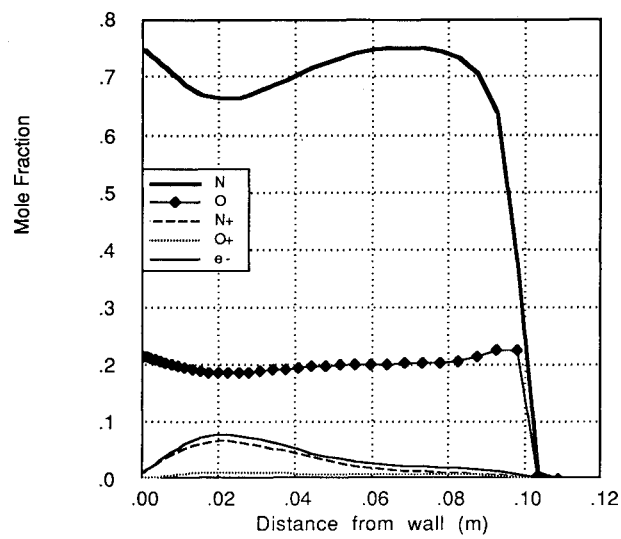

d) Shoulder region species distribution

Fig. 2 Computed profiles, 13.2 km/s.

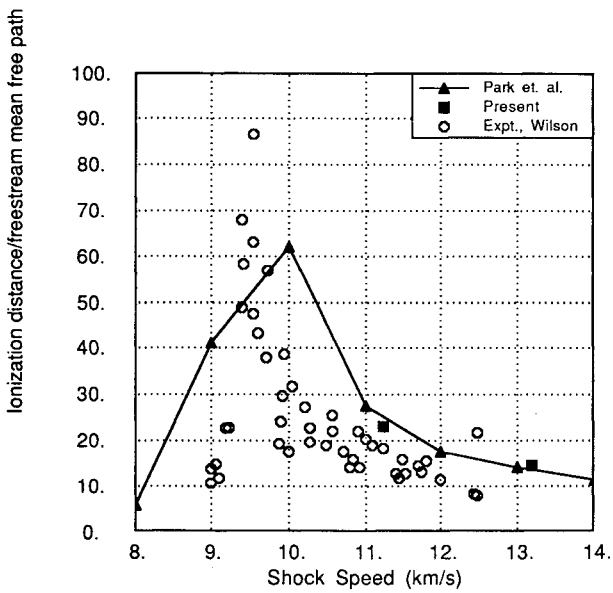

Fig. 3 Comparison of computed and experimental ionization distances.

fact that the flow solution is jumping grid lines. Along the stagnation line, the shock lies between the 36th and 38th grid line normal to the body. At the shoulder, the shock lies between the 30th and 32nd grid line. Therefore, at several places in the computational domain as the flow travels from the stagnation region to the shoulder, the shock wave jumps to a lower normal grid line. If this happens, inaccuracies are introduced into the evaluation of the thermoelectric term, and a lower level of self-generated magnetic induction is computed than should be. The use of adaptive grid techniques to align the grid to the shock would improve the quality of the solution by reducing or eliminating the incidence of the shock jumping grid lines.

Effects of an Applied Magnetic Field

The term $j \times B$ in Eq. (3) is the electromagnetic force term. When a strong magnetic field is applied, this term pushes the bow shock away from the body. Magnetic fields were applied to the aerobrake to gauge the effects on the flowfield. An axially symmetric externally applied magnetic field is considered. Two field strengths are considered, giving a magnetic induction value at the stagnation point of 0.05 and 0.1 T, respectively. Fig. 5 shows velocity contours with no applied magnetic field, and when a 0.1-T field is applied. There is a significant increase in shock standoff with the 0.1-T field,

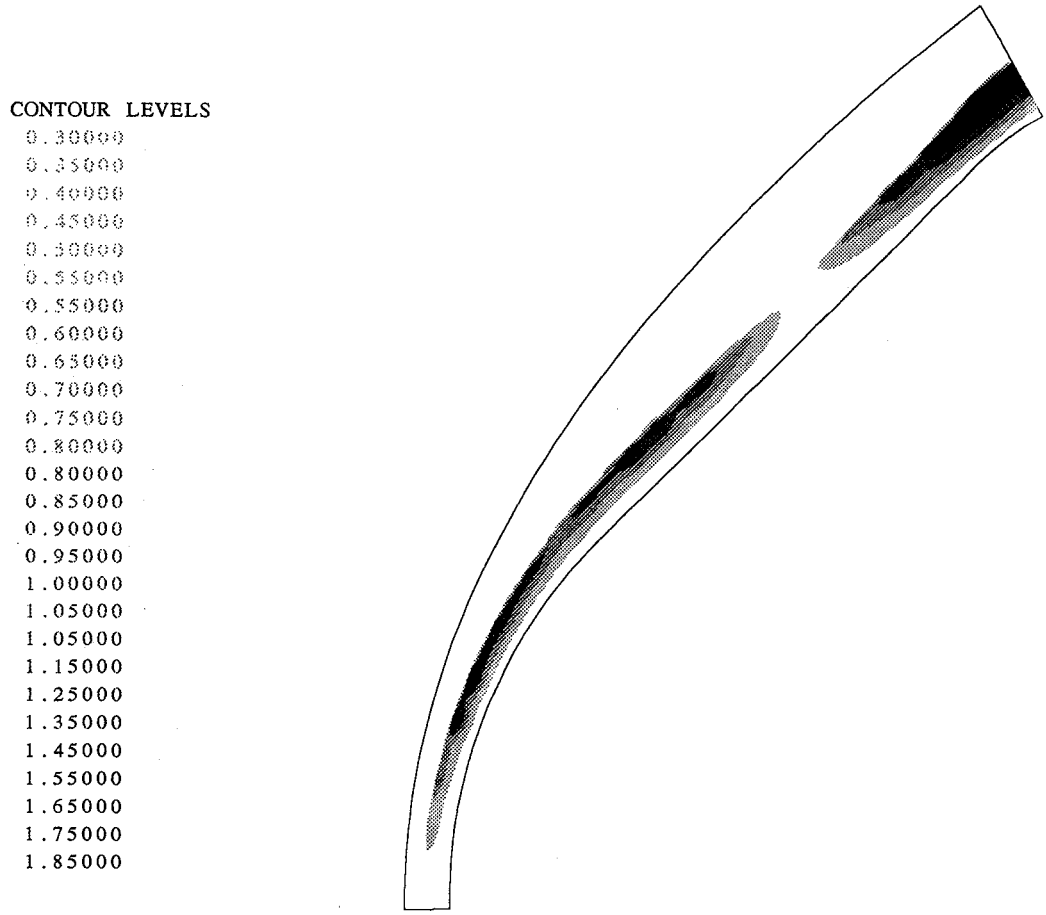

Fig. 4 Magnetic induction contours, G.

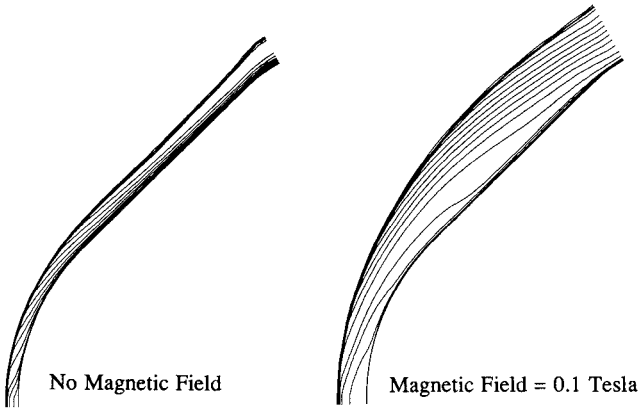

Fig. 5 Effects of an applied magnetic field on velocity contours.

which is a modest field strength easily acheived by either a permanent or solenoid-type magnet. The overall contribution to vehicle weight would be slight.

In Ref. 10, the effect of an applied magnetic field on the shock standoff distance was measured in a 3-in.-diam electromagnetic shock tube. The change in shock standoff was plotted as a function of $Q^* = B_0^2/\eta\rho_\infty U_\infty$ where B_0 is the value of magnetic induction at the stagnation point. The 0.05- and 0.1-T cases corresponded to Q^* values of 3.9 and 20, respectively. Figure 6 shows the values of the change of shock standoff found in this study vs the experimental and analytical values from Ref. 10. This comparison confirms the present technique's ability to correctly compute the change in shock standoff distance under the influence of an applied magnetic field. It also indicates that the effect of an applied magnetic field is not a linear function of the field strength, but is approximately a function of the square of the field strength.

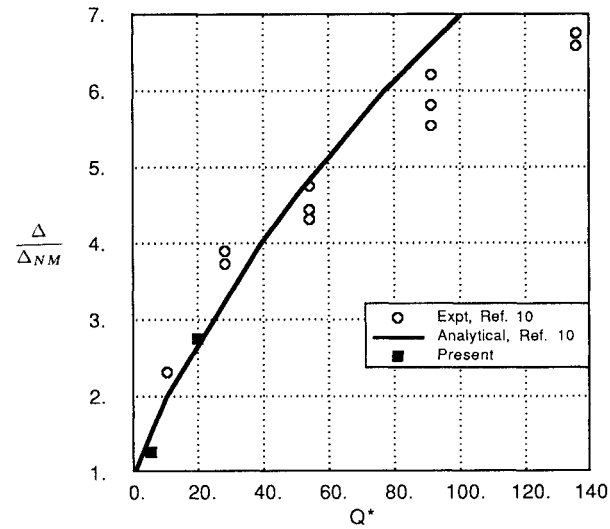

Fig. 6 Change in shock standoff distance.

Figure 7 shows stagnation line profiles of the two magnetic cases as well as the initial solution where no field is applied. The 0.05-T magnetic field had little effect on the flowfield, but the 0.1-T field had a pronounced effect. This is because while the 0.1-T field was only two times larger than the 0.05-T field, its Q^* value is five times larger. Figure 7a shows velocity profiles. Because the shock has been pushed away from the body, the normalized velocity gradient at the wall is reduced from 51.07 s^{-1} for no magnetic field, to 36.3 s^{-1} for the 0.05-T field, to only 7.41 s^{-1} for the 0.1-T stagnation point field strength. The reduction of velocity gradient at the outer edge of the boundary layer would reduce convective heat transfer.[11]

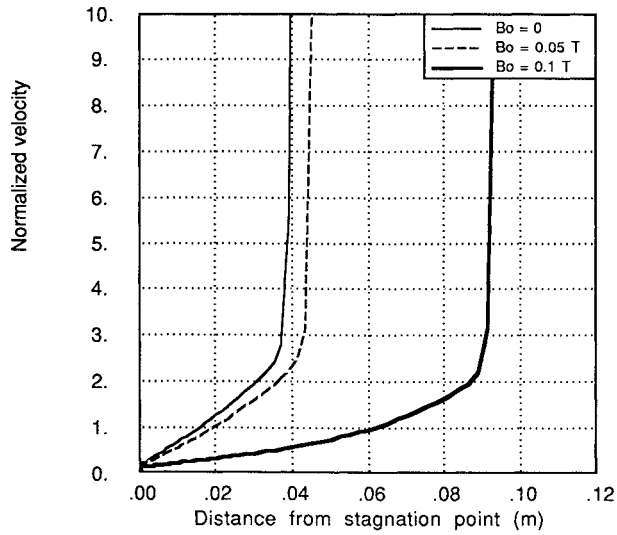

a) Velocity profiles

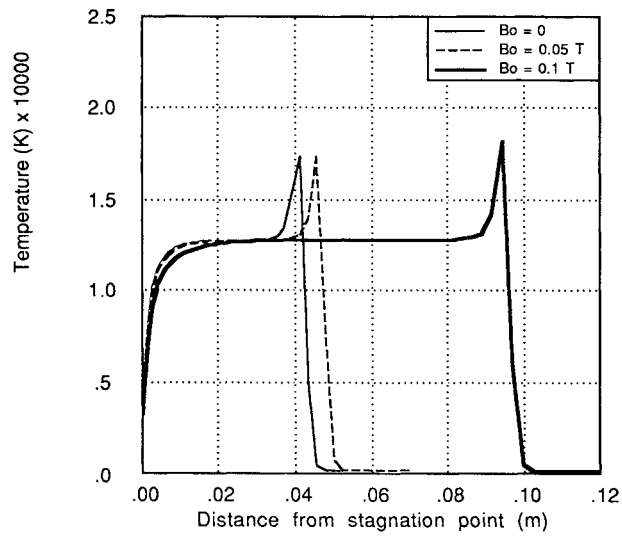

b) Temperature profiles

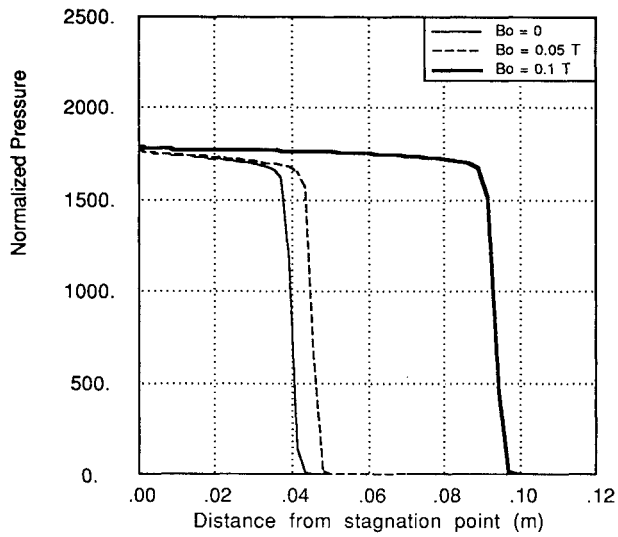

c) Pressure profiles normalized by $\rho_\infty c_\infty^2$

Fig. 7 Stagnation line profiles of two magnetic cases and an initial solution with no applied field.

Figure 7b shows stagnation line temperature profiles for the three cases. The peak temperature behind the shock and the equilbrium temperature throughout most of the shock layer are similar for all three cases. While the decreased temperature gradient at the wall for the 0.1-T case, as compared to when no field is applied, would indicate a reduction in convective heat transfer, the increased size of the high-temperature zone behind the shock would indicate an increase in the radiative heating to the body. Since the heat transfer at these flight conditions is expected to be radiation-dominated, the net effect with an applied magnetic field would be to increase the total heating rate.

Figure 7c shows the pressure profile along the stagnation streamline. The application of a magnetic field increases the pressure at the body, from an initial value of 1767–1769 for the 0.05-T case to 1782 for the 0.1-T case. This indicates that an applied magnetic field could be used as a control mechanism to alter the vehicle's L/D ratio or trim angle.

Similar effects on velocity gradient, surface pressure, and shock standoff distance from an applied magnetic field were found by Refs. 10–12 using analytic methods, Newtonian approximation, and experimental observations.

Concluding Remarks

The inclusion of electromagnetic effects introduces a strong stiffness into the system of governing equations. The explicit time-marching, first-order spatially accurate scheme developed in this article, overcomes this stiffness by loosely coupling the magnetic induction conservation equation to the other governing equations and using a very small time step when solving the induction equation. Flow was computed around a vehicle entering the Earth's atmosphere at a super escape velocity typical of a Mars return mission. When no external field is applied, the electromagnetic phenomenon cause little consequence to the fluid flow: the peak value of magnetic energy is seven orders of magnitude smaller that the total energy at the same grid point. The magnetic induction does not need to be coupled to the equation set. If it is desired, the self-generated magnetic field can be solved separately using the temperature and electron pressure obtained from the real-gas flow solver. Because the computation of a self-generated magnetic field relies on accurately resolving flow gradients in both coordinate directions, it is important to align the grid lines to the shock.

When an external magnetic field is applied to the ionized flowfield around a vehicle, the bow shock wave is pushed away from the body. The change in shock standoff distance is not a linear function of the field strength, but appears to be approximately a function of the field strength squared. A modest field of 0.1-T is sufficient to substantially increase the shock standoff distance of the Mars return aerobrake.

Under the influence of the applied magnetic field, the convective heating rate would decrease, but radiative heating would increase. The net effect would probably be to increase heating rates. An applied magnetic field could be used as a control mechanism to alter the vehicles L/D ratio or trim angle.

References

[1]Tauber, M. E., Palmer, G., and Yang, L., "Earth Atmospheric Entry Studies for Manned Mars Mission," AIAA Paper 90-1699, June 1990.

[2]Palmer, G., "Enhanced Thermochemical Nonequilibrium Computations of Flow Around the Aeroassist Flight Experiment Vehicle," AIAA Paper 90-1702, June 1990.

[3]Candler, G., "The Computation of Weakly Ionized Hypersonic Flows in Thermo-Chemical Nonequilibrium," Ph.D. Dissertation, Stanford Univ., Stanford, CA, June 1988.

[4]Gnoffo, P. A., Gupta, R. N., and Shinn, J. L., "Conservation Equations and Physical Models for Hypersonic Air Flows in Thermal and Chemical Nonequilibrium," NASA TP-2867, Feb. 1989.

[5]Ahluwalia, R. K., Vanka, S. P., and Im, K. H., "Three Dimen-

sional Analysis of MHD Generators: Development of Electrical Solution," AIAA Paper 81-0175, June 1981.

[6]Liu, B. L., Linberry, J. T., and Schmidt, H. J., "Three Dimensional Fluid and Electrodynamic Modeling for MHD DCW Channels," AIAA Paper 83-0464, Jan. 1983

[7]Liu, B. L., Schmidt, H. J., and Wu, Y. C. L., "Investigation of Non-Uniform Magnetic Field Effects on MHD Channel Performance," AIAA Paper 86-1058, May 1986.

[8]Shebalin, J. V., "Aerobrake Plasmadynamic Macroscopic Effects," AIAA Paper 90-1559, June 1990.

[9]Meyer, R. X., "Magnetohydrodynamic-Hypersonic Flow in the Quasi-Newtonian Approximation," *Reviews of Modern Physics*, Vol. 32, No. 4, 1960, pp. 1004–1007.

[10]Ziemer, R. W., and Bush, W. B., "Magnetic Field Effects on Bow Shock Stand-Off Distance," *Physical Review Letters*, Vol. 1, No. 2, 1958, pp. 58, 59.

[11]Bush, W. B., "Magnetohydrodynamic-Hypersonic Flow Past a Blunt Body," *Journal of the Aero/Space Sciences*, Vol. 25, Nov. 1958, pp. 685–690.

[12]Resler, E. L., and Sears, W. R., "The Prospects of Magneto-Aerodynamics," *Journal of the Aeronautical Sciences*, Vol. 25, No. 4, 1958, pp. 235–245.

[13]Levy, R. H, Gierasch, P. J., and Henderson, D. B., "Hypersonic Magnetohydrodynamics with or Without a Blunt Body," *AIAA Journal*, Vol. 2, No. 12, 1964, pp. 2091–2099.

[14]Kemp, N. H., "On Hypersonic Stagnation-Point Flow with a Magnetic Field," *Journal of the Aeronautical Sciences*, Vol. 25, June 1958, pp. 405–407.

[15]Lee, J. H., "Basic Governing Equations for the Flight Regimes of Aeroassisted Orbital Transfer Vehicles," Vol. 96, Progress in Astronautics and Aeronautics, AIAA, New York, 1985, pp. 3–53.

[16]Appleton, J. P., and Bray, K. N. C., "The Conservation Equations for a Nonequilibrium Plasma," *Journal of Fluid Mechanics*, Vol. 20, Pt. 4, 1964, pp. 659–672.

[17]Braginskii, S. I., "Transport Processes in a Plasma," *Reviews of Plasma Physics*, Vol. 1, Consultants Bureau, New York, 1965, pp. 205–292.

[18]Curtiss, C. F., and Hirschfelder, J. O., "Transport Properties of Multicomponent Gas Mixtures," *Journal of Chemical Physics*, Vol. 17, No. 6, 1949, pp. 550–555.

[19]Howe, J. T., "Hypervelocity Atmospheric Flight: Real Gas Flow Fields," NASA RP-1249, Nov. 1990.

[20]Gupta, R., Yos, J., and Thompson, R., "A Review of Reaction Rates and Thermodynamic and Transport Properties for the 11–Species Air Model for Chemical and Thermal Nonequilibrium Calculations to 30000K," NASA TM-101528, Feb. 1989.

[21]Park, C., Howe, J. T., Jaffe, R. L., and Candler, G. V., "Chemical-Kinetic Problems of Future NASA Missions," AIAA Paper 91-0464, Jan. 1991.

[22]Spitzer, L., *Physics of Fully Ionized Gases*, Interscience, New York, 1962, pp. 136–143.

[23]Delcroix, J. L., *Introduction to the Theory of Ionized Gases*, Interscience, New York, 1960, pp. 122, 123.

[24]Park, C., "A Review of Reaction Rates in High Temperature Air," AIAA Paper 89-1740, June 1989.

[25]Anderson, W. K., Thomas, J. L., and Van Leer, B., "Comparison of Finite Volume Flux Vector Splittings for the Euler Equations," *AIAA Journal*, Vol. 24, No. 9, 1986, pp. 1453–1460.

[26]Palmer, G. E., "An Improved Flux-Split Algorithm Applied to Hypersonic Flows in Chemical Equilibrium," AIAA Paper 88-2693, June 1988.

[27]Palmer, G., "The Development of an Explicit Thermochemical Nonequilibrium Algorithm and Its Application to Compute Three-Dimensional AFE Flowfields," AIAA Paper 89-1701, June 1989.

[28]Wilson, J. F., "Ionization Rate of Air Behind High-Speed Shock Waves," *Physics of Fluids*, Vol. 9, 1966, pp. 1913–1921.

[29]Park, C., "On Convergence of Computation of Chemically Reacting Flows," AIAA Paper 85-0247, Jan. 1985.